OPERATIONAL OCEANOGRAPHY AND METEOROLOGY

OC3570

WINTER 2004

CRUISE REPORT

Mass convergence from geostrophy and ADCP measurements

LCDR Patrice Pauly

French navy

Introduction

The oc3570 gives the students the opportunity to fit the theoretical studies with the oceanographer daily work. In spending half a week on board the research ship R/V “Point Sur”, we could have collected a large amount of data such as wind, temperature, salinity profiles, water samples and so on. Actually owned by the National Science Foundation, the “Point Sur” is operating for Moss Landing Marine Laboratories. This cruise was divided in two 4-day legs and data used for this topic are from the first one held in 27-30 January 2004. During the navigation, CTD data were acquired at 31 different stations grouped along three lines corresponding to lines 67, 70 and 77 of the California Cooperative Oceanic Fisheries Investigation (CalCOFI), forming what will be called the CenCal Box. Stations 1 to 10 correspond to CalCOFI line 67, stations 10 to 21 to CalCOFI line 70 and stations 21 to 31 to CalCOFI line 77.

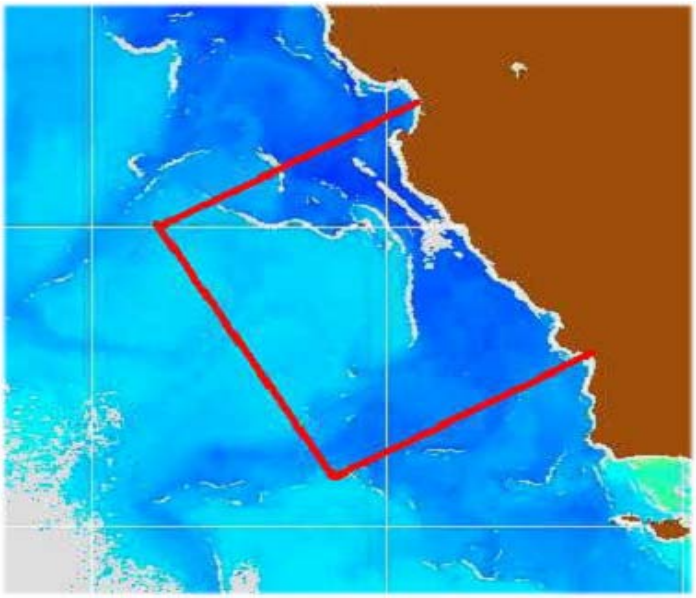

fig. 1: Cencal box

The purpose of this report is to compare computed geostrophic currents calculated from 35 conductivity, depth, pressure (CTD) casts, with currents measured by an Acoustic Doppler Current Profiler (ADCP). This data will also be compared to real-time TOPEX/ERS-2 satellite imagery, providing sea surface height anomaly. Thereby, geostrophic velocities will be used to compute volume transport in or out of the CenCal Box formed by the CTD sampling scheme. From

these computations, we will point out the mechanisms involved in mass transport and state on geostrophic method efficiency in computing mass transport.

The California current system

One usually classifies ocean currents by their driving mechanism, either wind driven or thermohaline. Thermohaline refers to differences in temperature and salinity which mainly drive the intermediate, deep and bottom circulation. The wind driven circulation runs most of the surface circulation. These wind driven currents are organized into a series of gyres in each of the ocean basins overlaying large scale wind systems.

The large-scale atmospheric forcing in the eastern Pacific Ocean consists of the North Pacific (sub-tropical) high and the Aleutian low. These forces create the anticyclonic (clockwise) North Pacific Subtropical Gyre, which includes the North Equatorial Current (NEC), Kuroshio Current, North Pacific Current (West Wind Drift) and the California Current System (CCS) as shown in figure 1.

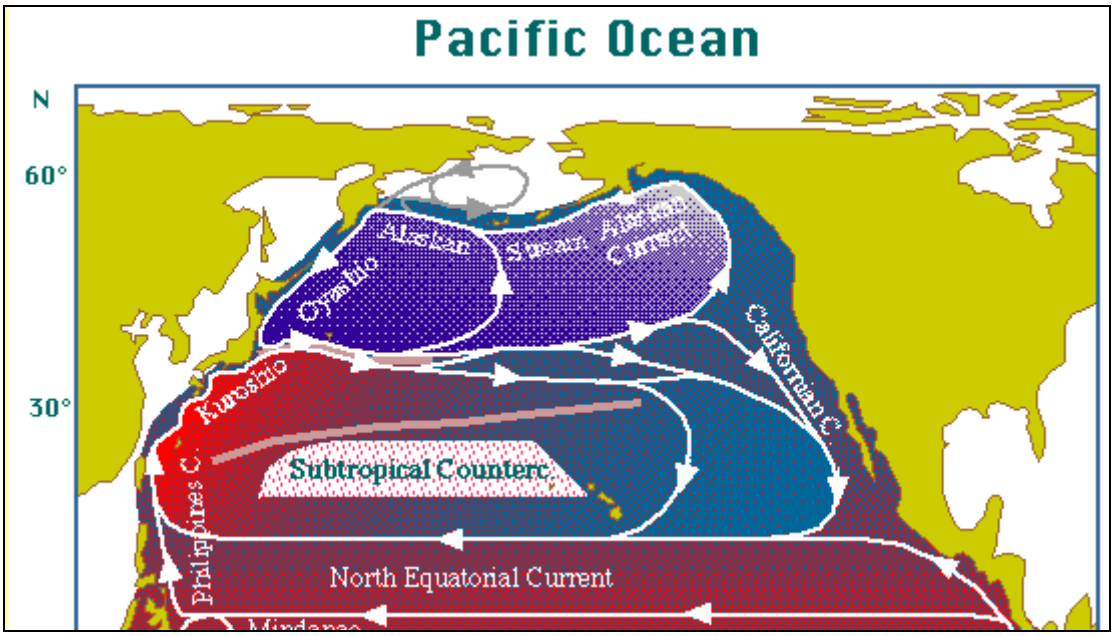

Fig. 2: North Pacific Subtropical Gyre

The CCS forms the eastern branch of the North Pacific Subtropical Gyre, flowing equatorward from southern Canadian coastlines down to northern Mexico. Between the Strait of Juan de Fuca (Canadian border) and Point Conception (west of Santa Barbara), the CCS can usually be separated into three large-scale (> 500 km) alongshore currents: the California Current (CC), the Davidson Current (DC), and the California Undercurrent (CUC) (Hickey, 1998).

- The CC is a surface (0-300 m deep) current 300-400 km offshore, carrying cold, fresh subarctic water southward with average speeds generally less than 25 cm/s (Reid and Schwartzlose, 1962).
- The CUC flows poleward over the continental slope from Baja (Mexico) to at least 50º N with a relatively narrow width between 10-40 km (Hickey, 1998). Taking its origin in the eastern equatorial Pacific, it is identified by a warm, saline and nutrient-poor signature. His maximum speeds are about 30-50 cm/s occurring between 100 and 300 m and can be observed at times over distances of 400 km and more (Collins et al., 1996).
- The DC is a seasonal surface current, flowing poleward during the fall and winter over the shelf from Point Conception to Vancouver Island (Canada). Measurements in the region have shown that the seasonal cycle over the slope is changing with the poleward flow, maximum usually occurring in May (Collins et al., 1996). The reversal of winds from northwesterly in summer to southeasterly in winter, which causes downwelling at the coast, seems to be the forcing mechanism of this poleward surface current (Huyer et al., 1989). It has also been suggested that the DC is a result of the surfacing of the CUC during late fall (Pavlova, 1966; Huyer and Smith, 1974).

Downwelling and upwelling conditions

Between approximately 35° and 50°N (Monterey Bay is at 36.6°N), wind forcing is determined by both positions and intensities of the North Pacific High and Aleutian Low Pressure systems. As the coastline is primarily oriented N-S, and

the winds are mainly alongshore, Ekman transport acts to create a vertical motion.

- During winter time, standard winds blow poleward north of 38°N, currents on the shelf are toward the north (Davidson Current) and downwelling conditions occur, although the core of the California Current still flows to the south further offshore.
- Through the year, as equatorward winds are prevailing, upwelling of deeper waters occurs to replace the surface waters displaced offshore.

METHOD

Abstract

Geostrophic flow is the name given to a current system that develops as a result of an elevated portion of the ocean sitting on a rotating earth. In the central gyres (for example, North Pacific Subtropical Gyre) where seawater is heated, the relative “sea level” in a steady state situation results in a “hill”. Of course, water at the “top of the hill” will flow down because of gravity. But the "hill of seawater" is on a rotating earth so as the water flows down it will be deflected to the right (in the northern hemisphere): that is what we call geostrophic flow. As the system is considered in steady state, this geostrophic flow results in a steady clockwise gyre. They are "calculated currents". A physical oceanographer determines the “elevation” of water from knowledge of the specific volume (inverse of density) of seawater. The elevation is based on a reference depth where density or specific volume is nearly constant on an ocean-basin size basis.

Mathematics

The geostrophic method to compute velocity is based upon the mathematical expression:

$$V\,2\Omega\sin\varphi = -\frac{1}{\rho}\frac{\partial\rho}{\partial x}$$

where V = speed of flow, Ω = angular speed of rotation of the earth, φ = latitude, ρ = water density and $\frac{\partial\rho}{\partial x}$ = horizontal pressure gradient.

From both temperature and salinity measurements, we can deduct density, using equation of state:

$$\rho(S,T,p) = \frac{\rho(S,T,0)}{1 - p/K(S,T,p)}$$

where ρ(S,T,0) and K(S,T,p) are polynomial expressions[1].
For our purpose, we will use the linearized equation of state (cf. annex 2).

In knowing only the pressure gradient, derived from the density distribution, one can compute the geostrophic currents. The first way to get pressure field is to measure it at different levels but we commonly use the dynamic topography, field of dynamic heights, induced by the density differences between two locations.
These geopotential heights will characterize equal pressure surfaces and so describe the pressure gradient.
The geostrophic currents are resulting from the balance between the pressure gradient force and the Coriolis force which acts all moving bodies. As a result, in the northern hemisphere, the water will be flowing keeping the higher sea surface (lighter water) on its right.
Nevertheless, this method only gives relative currents. We need a reference level at which the current is zero, or at least assumed to be. This so-called level is the level of no motion. Commonly chosen at 1000m, a former study in that region

1 UNESCO international equation of state 1980.

showed 250m to be a greater option[2]. But this one was based upon summer data. Even if, we will check both values,

1000m will be the initial choice for level of no motion.

As the height of the upper isobaric surface will depend upon the whole water column, we need to integrate from the level of no motion (current supposed to be nil underneath) and the surface or the depth we want to compute the current at.
The quantity used for shaping is the standard geopotential distance defined by:

$$\Delta\Phi = \int_{P_1}^{P_2} \delta dp$$

where $\delta(S,T,p)$ is the specific volume anomaly.

The geostrophic velocity at one level V_1 relative to a lower level V_2 between two stations denoted by A and B is then estimated by

$$V_1 - V_2 = \frac{\left(\Delta\Phi_B - \Delta\Phi_A\right)}{2d\Omega Sin\phi_{ave}}$$

where d is the distance between both stations A and B and Φ_{ave} is the mean latitude.

In our purpose, the SeaWater subroutines[3] have been used to compute density, distances between stations, geopotential anomalies and geostrophic velocities using data of the CTD casts.

2 Juan Conforto, 2003 summer cruise report

3 Phillip P. Morgan, 1994. SEAWATER: A Library of MATLAB® Computational Routines for the Properties of Sea Water.

Geostrophic current from CTD measurements

Each station measurements provided temperature, salinity and pressure profiles.

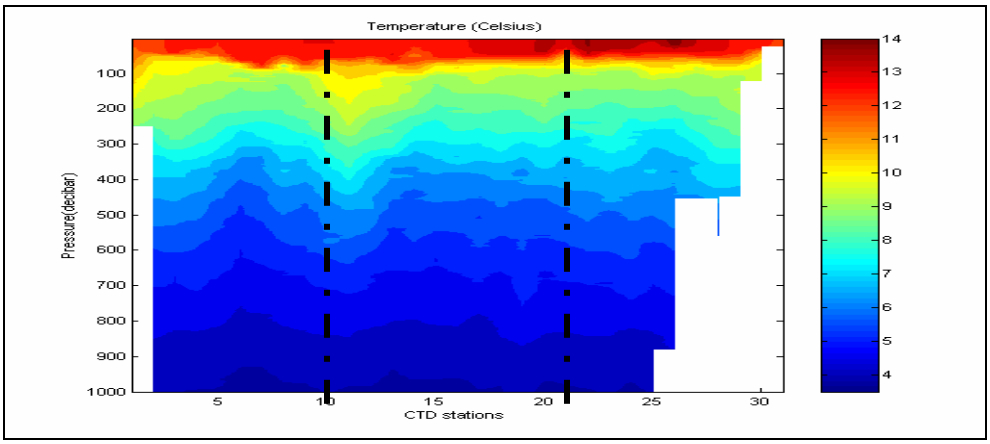

fig. 3: temperature distribution alongside the box

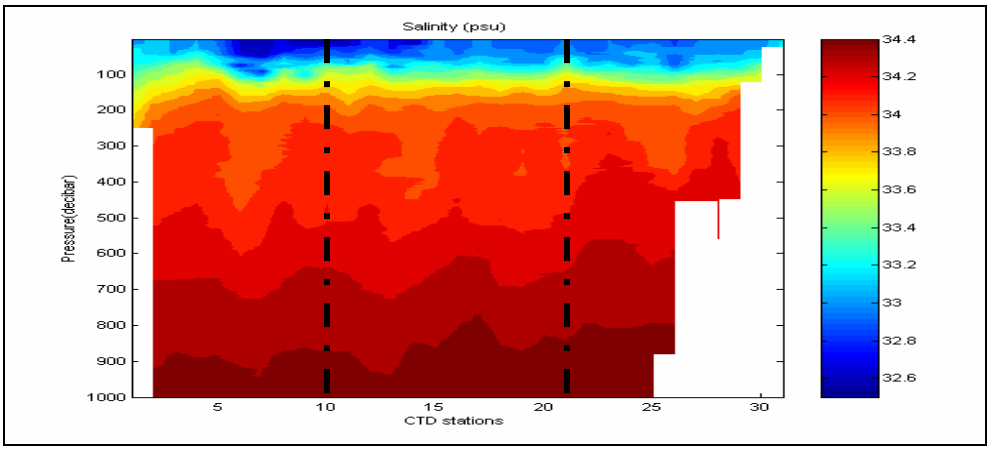

fig. 4: salinity distribution alongside the box

From these data, the geopotential anomaly has been computed using the MATLAB subroutine sw_gpan.m.

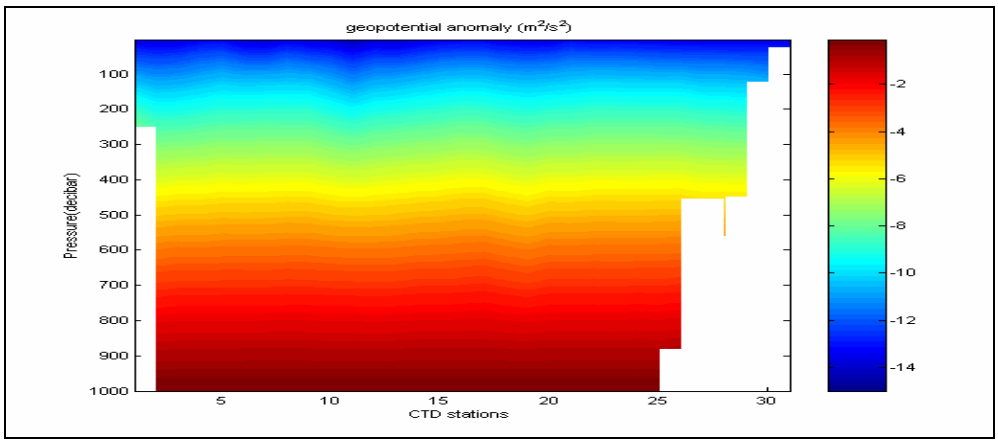

fig. 5: geopotential anomaly distribution alongside the box

The sw_gvel.m MATLAB subroutine allowed us an easy geostrophic velocity computation, setting the level of no motion to be at 1000m. As a result, we obtained:

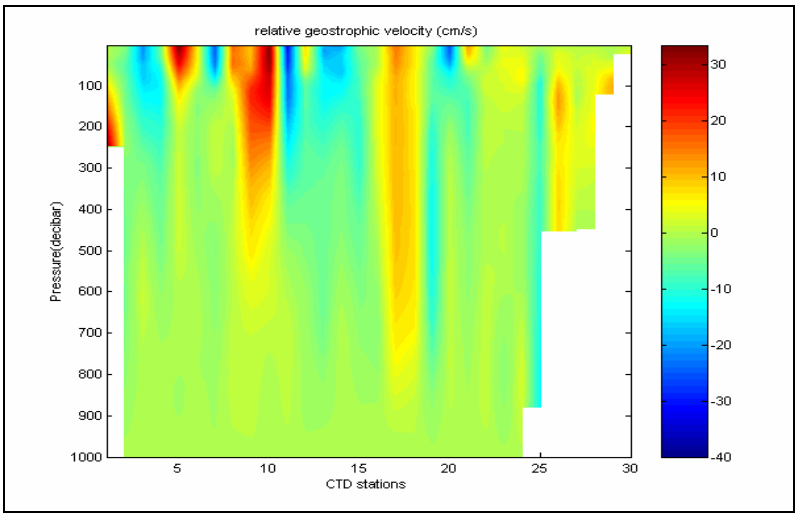

fig. 6: relative geostrophic velocity alongside the box

We must remain that all the computed current values are relative to the one observed at 1000m. At that point, there is no way to known whether our statement is valid or not.

The other point to underline is that this current is tilted across the track (positive values inward the box, the negative ones outward).

Current from ADCP measurements

But, instead of choosing an arbitrary level of no motion, we can also pick up as reference depth a depth where the current has been known.

The ADCP instrument recorded the along-track and across-track water velocities. These data should provide the real current values every 10 m depth down to 450m. The next two plots show how current is distributed along and across the track.

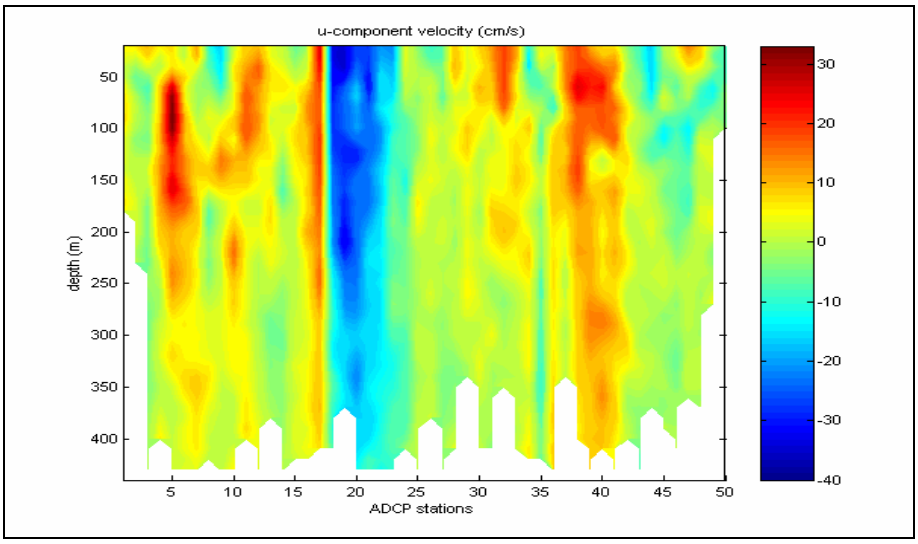

fig. 7: current speed alongside the box from ADCP measurements

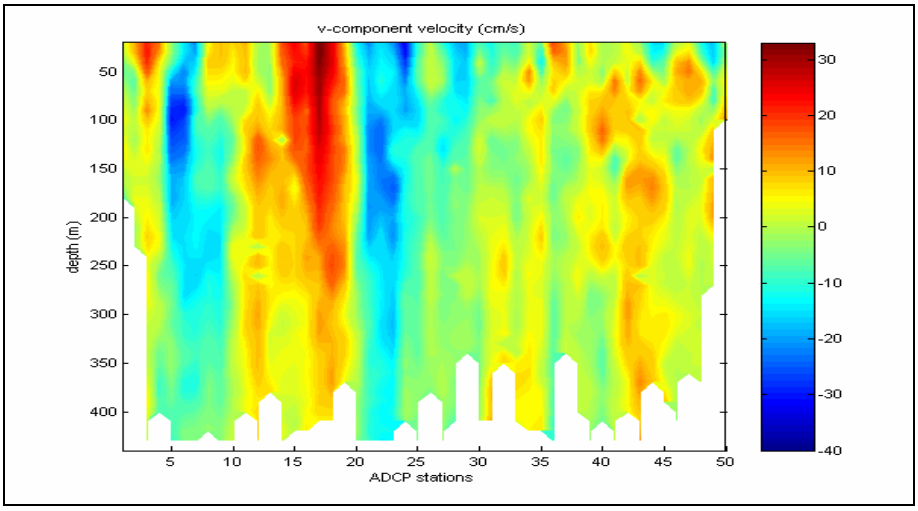

fig. 8: current speed across the box from ADCP measurements

The values we are really interested in are the across-track ones (v-component) which characterize the inflow or the outflow.

Even if we can identify the key features in the CTD-based plot, the difference with the ADCP-based is important and would lead to a great volume error computation.

Data comparison

To compare the two data sets, we have first to face a critical problem. The ADCP data were not collected at CTD station locations. As we have more ADCP measurements (51) than CTD stations (31), the comparison was made between both extrapolating ADCP records at CTD stations. This extrapolation uses a linear interpolation MATLAB routine.

The first plot shows the difference between ADCP values and a level of no motion set at 1000m.

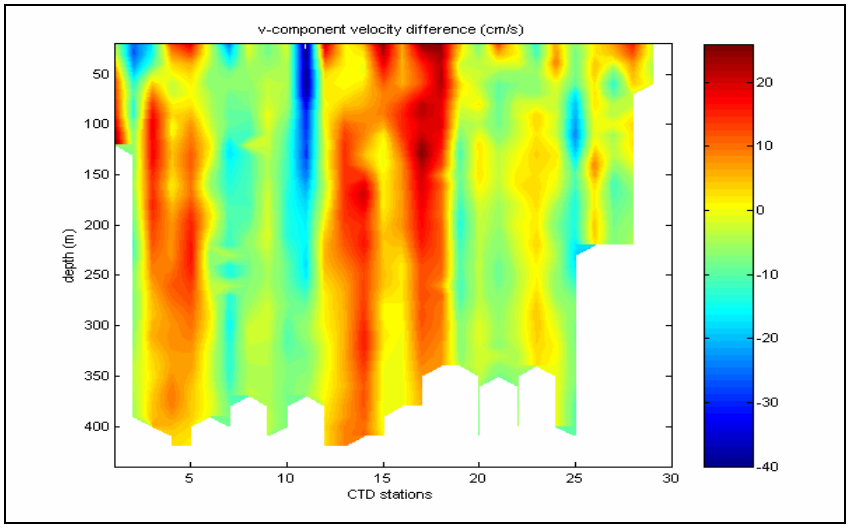

fig. 9: velocity difference across the box between CTD and ADCP measurements with level of no motion at 1000m

The differences between the CTD measurements and the ADCP are too large to reasonably consider the 1000m depth as a good level of no motion. Even if we guessed some differences in the mixed layer, the values should be very close underneath. We need to take another reference value.

To build up the next one, the 250m ADCP measurements stands for the reference value. Even if this choice was made during the last summer study, it was practically mandatory. We could not really take a deeper depth which would have dropped the last six stations out.

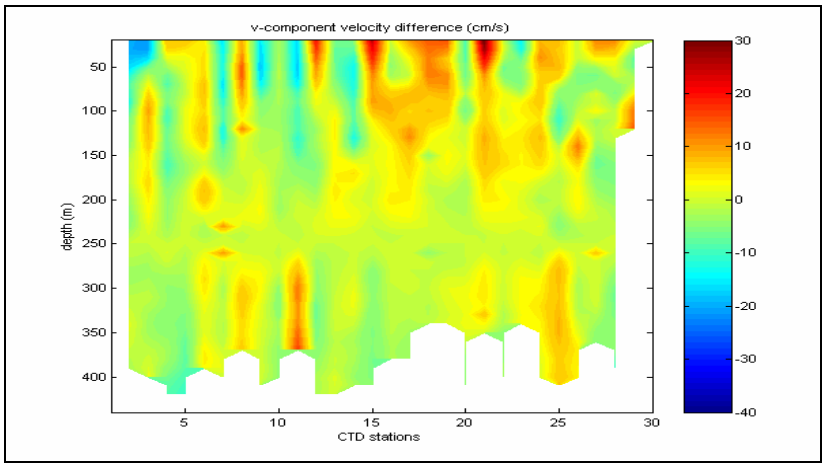

fig. 10: velocity difference across the box between CTD and ADCP measurements with reference level at 250m-ADCP measurement

More interesting is the fact that during legs 1 (from stations 1 to 11) and 3 (after station 21), CTD current calculations undervalue the ADCP measurements meaning the real flow entering the box is underestimated. During leg 2, the ADCP measurements give lower values showing the geostrophic method overestimate the total flow.

The resulting plot has values very close to zero around and underneath the reference level. Nevertheless, we can observe some important variations in the upper layer. In fact, the geostrophic balance is not the only force acting the surface layer. Motion due to tides or Ekman transport, due to the wind, can be very influential, even prevailing in case of strong winds.
These new values provide the starting point to the mass transport computation.

All the above computations are based upon measured data such as temperature or currents. The TOPEX – POSEIDON satellite can also provide these data to state whether or not our data are accurate enough.

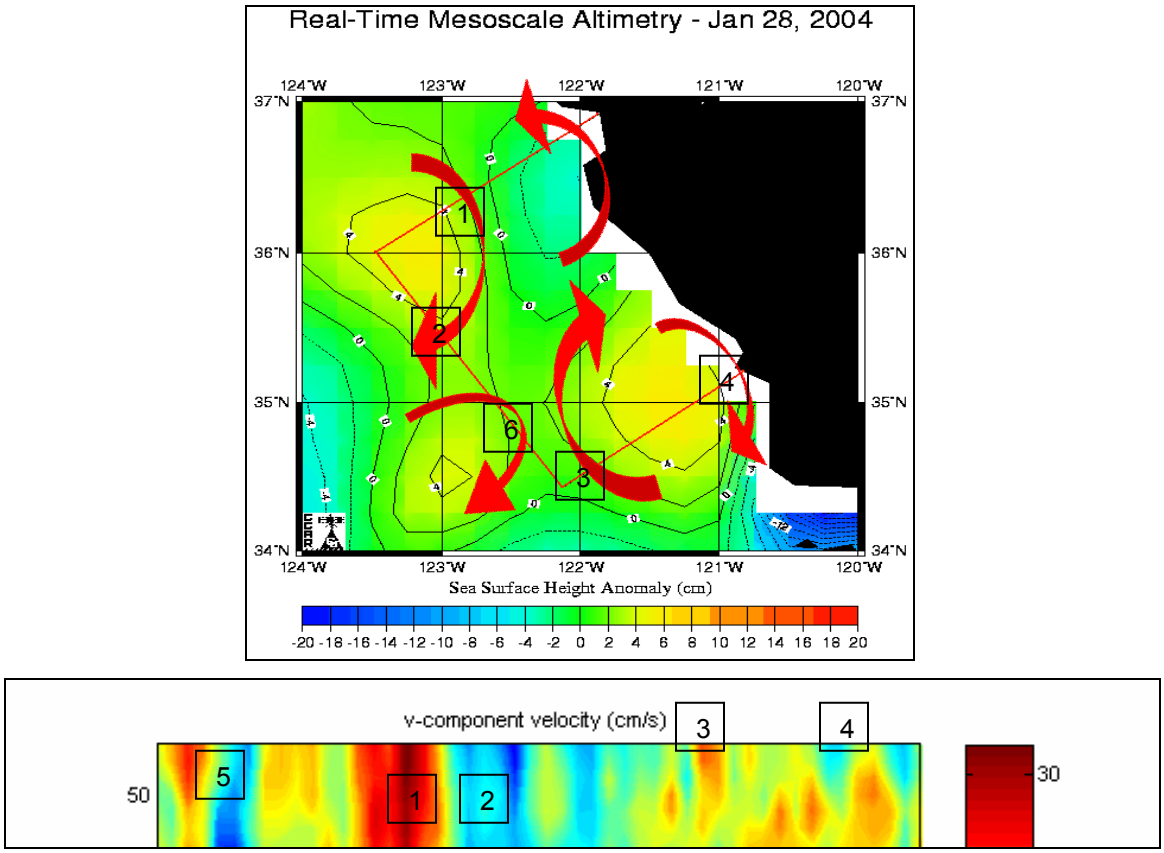

fig. 11: dynamic topography from TOPEX-POSEIDON (01/28/04)

The dynamic topography measured by satellite shows a rather flat surface with two small gyres close to the first turning point and in the middle of the last leg. The arrows show the direction of the geostrophic flow.

A rapid comparison between the satellite data and the ADCP measurements show that, even though the gyres are not very strong, the main flows have been observed. For effortlessness, I labeled with numbers both plots.

All features labeled 1 through 4 are seen on the two plots.

The depressive gyre (counterclockwise) located at the beginning of leg 1 has not been seen. Moreover, we observed a clockwise gyre (#5).

On the satellite plot, the gyre number 6 has not absolutely been seen. Nevertheless, we can set that the tiny change lying between # 2 and 3 can somehow characterize this gyre which is not very strong and whose isolines are parallel to the track line.

As a conclusion, the more remarkable observation we can make is that, although the gyres were weak, we observed with some accuracy what was going on.

Geostrophic volume transport

Once the geostrophic current has been computed, computing the volume transport only requests the knowledge of the section it will pass through. As we know this current for all section between two consecutive CTD stations, the total flow between two following stations requests the integration of the across-speed from surface down to 1000 meters (we considered no flow underneath). This total transport is expressed in m^3/s. In order to fit with oceanography literature, it will be expressed in Sverdrup (1 Sv = 10^6 m^3/s).

Then summing this flow for each leg will provide a mass transport value across legs 67, 70 and 77.

The final result lies in the next plot.

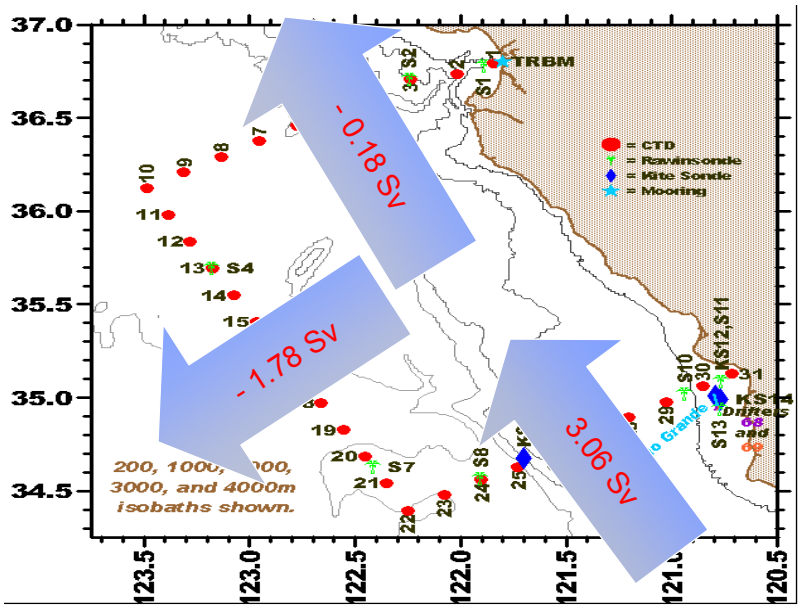

fig. 12: mass transport

From our calculation, the total mass transport equals +1.10 Sv, meaning there is more water entering the box than going out. There are couple of reasons for that.

The first one is that we neglected the flow beneath 1000 meters, which, even weak, is not null. The second reason stands in what we called v-component velocity difference we did not take into account. So the same computation was made with the remaining v-value.
As a result, we obtained that we neglected +0.14 Sv, meaning there is even more flow entering the box.
Finally, the total amount of water entering the box is +1.24 Sv.

But as we can easily state there is no flow through the coastline neither from it, and neglecting the rain fall, the total flow across legs 67, 70 and 77 should vanish as a result of conservation of mass.

Thus, a first explanation is that the remaining amount of water must cross the box between 1000 meters and the bottom. That can easily be shown looking at mass transport between each water column.

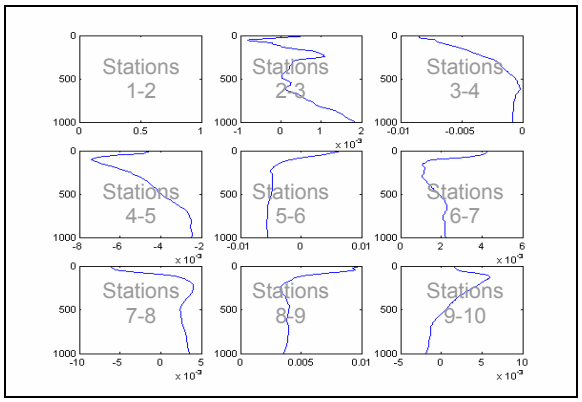

fig. 13: mass transport (mSv) on leg1

On leg 1, we can observe that, at 1000m, the flow is not negligible everywhere, specially between stations 2 and 3, 4 and 5, and 2 and 7. Considering these three columns, the total inflow is about 2.5 mSv/m.

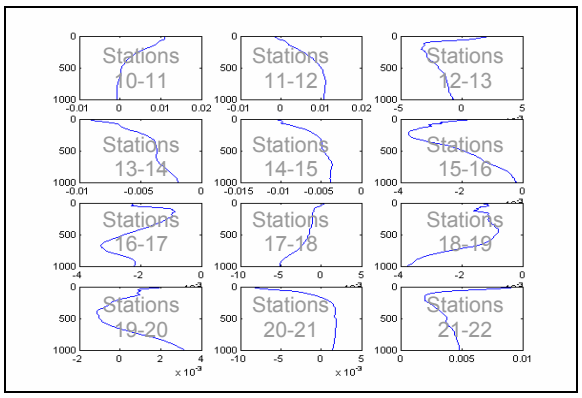

fig.14: mass transport (mSv) on leg2

With the same observations, the total outflow resulting from water columns between stations 16 and 21 equals -6 mSv/m. Moreover, during that leg, the bottom is deeper than during the first one.

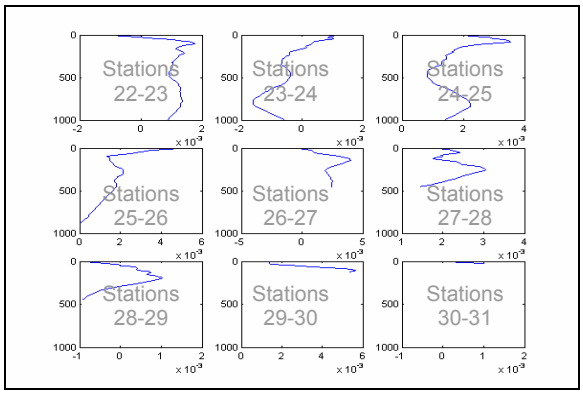

fig.15: mass transport (mSv) on leg3

The same way of thinking provides an inflow of 2 mSv/m during leg 3.

Finally, we end up with an additional outflow of -1.5 mSv/m. Assuming a reasonable mean bottom value at 2000 m, we lastly neglected 1.5 Sv, which is more or less the amount we initially computed.
But we must keep cautious. The last three plots show that the current is all but uniform within a water column.

A second way to explain the +1.24 Sv, is given by the regional oceanography. During winter time, downwelling conditions occur due to a mean northward wind. During, that cruise, weak winds had been blowing northeast for a while until the 27th then turned southeast. But downwellings do not vanish instantaneously. A mean value of 5 m/s wind speed ended up with an Ekman transport of 0.4 Sv, which did not balance the missing water but must partially be taken into account.

Conclusion

In fact, both downwelling and mass transport beneath 1000m must be valid and both effects should have provided a part of this remaining flow. But the geostrophic velocity method afforded a rather accurate result as long as the reference level was correct. In this particular example, the widespread 1000m level of no motion was not.
In one way or the other, the amount of water crossing the box was 34 Sv. Hence, the geostrophic method provided an accurate result with a 3% error. The presence of downwellings influenced the results. In fact, this method gave us the opportunity to point out local features such as undercurrents or up or downwellings.
So, this method should provide an even better result in a large offshore box.

ANNEX 1

Abreviations (in order of apparition)

Abbreviation	meaning	[unit]
S	salinity	[psu]
T	temperature	[ºC]
P	pressure	[bar]
ρ(S,T,p)	density of sea water	[kg/m^3]
ρ(S,T,0)	density of sea water at one standard atmosphere	[kg/m^3]
K(S,T,p)	secant bulk modulus	[bar]
Ω	angular speed of rotation of the earth (7.29 10^{-5})	[s-1]
V	speed of flow	[m/s]
φ	geographic latitude	[º]
ΔΦ	standard geopotential distance	[m^2/s^2]
δ(S,T,p)	specific volume anomaly	[m^3/kg]

ANNEX 2

$\rho(S,T,p) = RST_0 / (1-p/AK)$

$RST_0 = R_0 + AS + BS^{3/2} + CS^2$

$AK = A_1 + A_2 * S + A_3 S^{3/2} + (A_4 + A_5 S + A_6 S^{3/2}) P + (A_7 + A_8 S) P^2$

Where

$R_0 = 999.842594 + 6.793952e^{-2}T - 9.095290e^{-3}T^2 + 1.001685e^{-4}T^3 - 1.120083e^{-6}T^4 + 6.536336e^{-9}T^5$

$A = 8.24493e^{-1} - 4.0899e^{-3}T + 7.6438e^{-5}T^2 - 8.2467e^{-7}T^3 + 5.3875e^{-9}T^4$

$B = -5.72466e^{-3} + 1.0227e^{-4}T - 1.6546e^{-6}T^2$

$C = 4.8314e^{-4}$

$A_1 = 19652.21 + 148.4206T - 2.327105T^2 + 1.360477e^{-2}T^3 - 5.155288e^{-5}T^4$

$A_2 = 54.6746 - 0.603459T + 1.09987e^{-2}T^2 - 6.1670e^{-5}T^3$

$A_3 = 7.944e^{-2} + 1.6483e^{-2}T - 5.3009e^{-4}T^2$

$A_4 = 3.239908 + 1.43713e^{-3}T + 1.16082e^{-4}T^2 - 5.77905e^{-7}T^3$

$A_5 = 2.2838e^{-3} - 1.0981e^{-5}T - 1.6078e^{-6}T^2$

$A_6 = 1.91075e^{-4}$

$A_7 = 8.50935e^{-5} - 6.12293e^{-6}T + 5.2787e^{-8}T^2$

$A_8 = -9.9348e^{-7} + 2.0816e^{-8}T + 9.1697e^{-10}T^2$

References

Books:

Pond, S., and Pickard, G.L., *Introductory Dynamical Oceanography*, 2nd ed., pp 68-87, Butterworth/Heineman, 1983.

Pickard, G.L., and W.J. Emery, *Descriptive Physical Oceanography*, *An Introduction*, 5th ed., pp 95-120, Pergamon, 1990.

Computer facilities:

Phillip P. Morgan, 1994. SEAWATER: A Library of MATLAB® Computational Routines for the Properties of Sea Water. CSIRO Marine Laboratories Report 222. 29 pp.

Web sites:

Colorado Center for Astrodynamics Research, "Global Near Real-Time Altimeter Data Viewer" [http://www-ccar.colorado.edu/~realtime/global-real-time_ssh/] August 2003.